Catal Lett (2008) 125:359–370
DOI 10.1007/s10562-008-9459-8

Mesoporous Silica–Zirconia Systems for Catalytic Applications

E. Ghedini · M. Signoretto · F. Pinna · G. Cruciani

Received: 13 December 2007 / Accepted: 5 March 2008 / Published online: 13 September 2008

Abstract In this study synthesis and characterization of solid acid catalysts with definite textural properties (high surface area, narrow pore size dimension, ordered structure) are described. In particular sulphated zirconia (SZ) has been introduced on three ordered mesoporous silica, MCM-41, MCM-48 and SBA-15, in order to study the influence of silica supports on textural and chemical–physical properties of final catalysts. The correlation between the catalytic behavior of SZ supported samples and their textural and chemical physical properties was studied in the liquid-phase acylation of anisole with benzoic anhydride.

Keywords Mesoporous materials · Solid acid catalysts · Texture · Acylation

1 Introduction

The discovery of ordered mesoporous silica, of M41s types [1], in the early 1990s has attracted a great interest in many areas of physical, chemical and engineering sciences. The synthesis of these materials involves the use of a self-assembled molecular array of surfactants molecules as structure-directing agent. The removal of these templates led to very ordered mesoporous molecular sieves with adjustable pore sizes ranging from 2 to 10 nm [1]. Depending on the synthesis conditions, the silica source or the type of surfactants (ionic, non-ionic, co-polymer) used, different phases can be distinguished: MCM-41 (hexagonal), MCM-48 (cubic), SBA-15 (hexagonal) and other species. Owing to their special pore properties these materials can been exploited in systems where molecular recognition is needed: selective adsorption and separation process, chemical sensors, nanotechnology and shape-selective catalysis. In particular, the advantages of using ordered mesoporous solids in catalysis are the relatively large pores which facilitate mass transfer and the very high surface area which allows a high concentration of active sites per mass of material. In fact, a good heterogeneous catalyst must possess, besides active catalytic sites, a pore structure capable to host large reagents and to allow the formation of the desired product. Mesoporous silica are not often used as catalysts as such much more frequently catalytic functions are introduced by incorporation of active sites in the silica walls or by deposition of active species on the inner surface of the material. There are many possible pathways to modify mesoporous materials when one wants to give them a new catalytic function: grafting, immobilization of functional group, surface coating, ion exchange. The active sites can be constructed both directly or via post-synthesis procedures, which means that the properties of these active sites are variable and controllable, depending on the synthetic procedure.

In order to obtain a solid catalyst characterized by high surface area, ordered pore structure and active in acid catalyzed reactions, in this study ordered silica mesoporous materials have been modified with the introduction of sulphated zirconia (SZ) in their structure. Sulphated zirconia (SZ) is a solid acid catalyst that has been shown to be

E. Ghedini (✉) · M. Signoretto · F. Pinna
Department of Chemistry, University of Venice, Consortium INSTM, Research Unit of Venice University, Calle Larga St. Marta 2137, 30123 Venice, Italy
e-mail: gelena@unive.it

G. Cruciani
Earth Science Department, University of Ferrara, Via Saragat 1, 44100 Ferrara, Italy

active by a number of reactions like isomerization [2, 3], cracking [4], alkylation [5], acylation [6–8] and so on. When SZ is synthesized by a conventional method is very difficult to control its textural properties and large pore are formed with wider pore size distribution. So, the use of mesostructured materials, which have uniform mesopores and very high surface area (typically around 900–1,000 m^2/g or higher), as a catalyst support for SZ, should greatly expand the catalytic property and capabilities of SZ for some applications.

Insertion of pure zirconia [9–12] and of sulphated zirconia [13–18] on mesoporous materials, especially on MCM-41, have been reported by several groups and all these procedures allow obtaining materials with relatively high surface areas and narrow pore size distribution. In a recent work [19] we showed that is possible to obtain very ordered metal promoted SZ/MCM-41 systems active in gas and liquid phase reactions of industrial interest.

The goal of our work was therefore to synthesize mesoporous solid acid catalysts with tailored textural properties by introducing SZ on three different ordered silica materials. We have used as supports: MCM-41 [1], MCM-48 [20] and SBA-15 [21], in order to evaluate the effect of textural and chemical–physical properties of silica on characteristics of final catalysts.

The benzoylation reaction of anisole was used as a test reaction to evaluate the potential application of our systems as catalysts in liquid-phase acylation reactions of aromatics.

The correlation between the catalytic behaviors of SZ supported systems and their different textural and chemical physical properties had been discussed.

2 Experimental

2.1 Synthesis of Supports

MCM-41 silica was synthesized according to procedure reported in a previous work [19].

The MCM-48 was synthesized following the method reported by Monnier et al. [20].

SBA-15 was prepared with TEOS as the silicon source and EO20-PO70-EO20 (P123) (ALDRICH) as the template in an aqueous HCl solution, according to Zhao et al. [21].

Introduction of Sulphated Zirconia on silica supports was carried out as previously reported [19] by incipient wetness impregnation of $Zr(SO_4)_2$ in the as-synthesized supports, followed by thermal decomposition of precursor in flowing air.

The calcined samples were designated as SZX with SZ standing for sulphated zirconia and X for M41 (MCM-41), M48 (MCM-48), SBA (SBA-15) respectively.

2.2 Characterization

Surface area and pore volume were obtained from N_2 adsorption-desorption isotherms at 77 K (MICROMERITICS ASAP 2000 Analyser). Prior to the sorption experiment, the materials were dehydrated by evacuation at 383 K for 2 h. Mesopore volume, $V_{mes,}$ was measured as the adsorbed amount of N_2 after capillary condensation, micropore volume, $V_{micopor}$, was obtained by *t*-plot method.

XRD powder diffraction pattern of the samples were obtained on a Philips PW 1820/00 instrument with Cu Kα radiation at 40 kV and 30 mA.

Surface area was calculated from the adsorption branch by the BET equation [22], whereas the mesopores diameter, $D_{mes\ +\ XRD}$, was determined by a geometrical method (from adsorption and crystallographic data) taking into account of the hexagonal and cubic shape of the pores [23, 24]. Cell size *a* and wall thickness *t* were calculated from XRD data. In the case of MCM-48 and SZM48, the equations used for the determination of pore diameter ($D_{mes\ +\ XRD}$) and of wall thickness from the lattice parameter are:

$$t = 0.3234a(1 - \varepsilon) \tag{1}$$

where

$$a = d_{211}\sqrt{6} \tag{2}$$

and

$$D = \frac{a}{2}[1 - 0.648(1 - \varepsilon)] \tag{3}$$

For the samples characterized by hexagonal structure, instead, the used equations are:

$$t = a - 0.95D \tag{4}$$

where

$$a = d_{100}\left(\frac{2}{\sqrt{3}}\right) \tag{5}$$

and

$$D = 1.05a\sqrt{\varepsilon} \tag{6}$$

The void fraction ε (ratio void volume/total volume for calcined materials) has been calculated as:

$$\varepsilon = \frac{V_{mes}}{V_{mes} + V_{SiO_2}} \tag{7}$$

Assuming a density 2.2 for the amorphous silica wall. The pore size distribution was determined by the BJH method applied to the N_2 adsorption isotherm branch.

Sulphate content was determined by a previously described ion chromatography method [25].

Transmission electron microscopy (TEM) images were taken with a Jeol 3010, operating at 300 kV equipped with a

GATAN slow-scan CCD camera (Mod. 794) and an Oxford instrument EDS microanalysis detector (Mod. 6636). Some powder from each sample was suspended in isopropyl alcohol, ultrasonicated for 5–10 min so that the particles were well dispersed and deposited on a holey carbon film.

FTIR spectra were obtained on a BRUKER 113v spectrophotometer (2 cm^{-1} resolution, MCT detector). SZ-based samples were inspected in the form of thin layer depositions ($\sim$10 mg cm^{-2}) on Si wafers, starting from aqueous suspensions. All samples were activated in controlled atmosphere at 473 K in quartz cells connected to a gas vacuum line, equipped with mechanical and turbo molecular pumps (residual pressure $P < 10$–5 Torr), which allows to perform strictly in situ adsorption/desorption experiments.

2.3 Catalytic Testing

The acylation reaction was carried out at 323 K in a thermostated batch reactor, using benzoic anhydride, FLUKA 99.0%, (0.0013 mol), anisole, FLUKA 99.9% (10 ml) and *n*-tetradecane, FLUKA 99%, employed as internal standard for GC. Before the introduction in the reaction medium, the catalyst (200 mg) was activated at 723 K in flowing air for 90 min and kept dry. Aliquots of the reaction mixture were taken periodically after 10, 20, 30, 60, 90, 120 and 180 min via syringe, filtered to separate the catalyst and analyzed by gas chromatography equipped with an HP-5 column and a FID detector.

Since anisole was in excess, conversion was based on the benzoic anhydride consumption (C_{AN0}–C_{AN}) and yield was calculated on the production of 4- and 2-methoxybenzophenone (2- and 4-MPB) isomers.

$$\text{Conversion}(\%) = \frac{C_{AN0} - C_{AN}}{C_{AN0}} \times 100 \quad (8)$$

$$\text{Yield}(\%) = \frac{C_{MPB}}{C_{AN0}} \times 100 \quad (9)$$

3 Results and Discussion

3.1 Textural and Chemical–Physical Properties

The morphology of obtained calcined samples was detected by N_2 physisorption. The loops of N_2 adsorption-desorption isotherms and the profiles of the pore diameter distribution are shown in Figs. 1 and 2 respectively. Pore size dimensions have been evaluated from a geometric method (from lattice dimensions and mesopores volume) following the equations reported in the previous section.

For MCM-41 and SZM41 samples the physisorption measurement follow the type IV isotherm (see Fig. 1a),

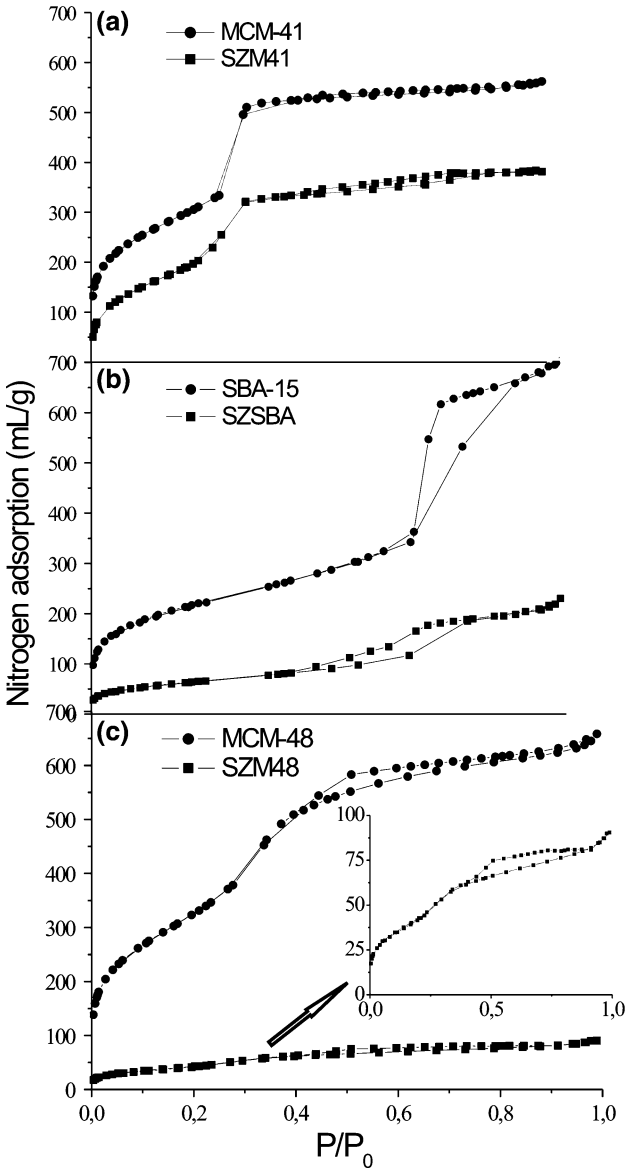

Fig. 1 N_2 adsorption/desorption isotherms of silica supports (MCM-41, MCM-48, SBA-15) and of SZ promoted systems: (**a**) MCM-41/SZM41; (**b**) SBA-15/SZSBA; (**c**) MCM-48/SZM48

without hysteresis between the adsorption and the desorption branches, in agreement with literature data [26] for materials with a similar pore size dimension ($\sim$3 nm). The isotherm of plain silica exhibit a significant adsorption at low relative pressure that is probably associated with the monolayer coverage of the pore walls by nitrogen; another well-defined step uptake between approximately P/P0 = 0.2–0.3 associated with the filling of the mesopores due to capillary condensation and its is followed by a plateau for P/P0 > 0.35. The sharpness of the second step reflects a narrow and uniform distribution of the pore size as confirmed by transmission electron microscopy (see Fig. 5). For SZ promoted system the amount of adsorbed

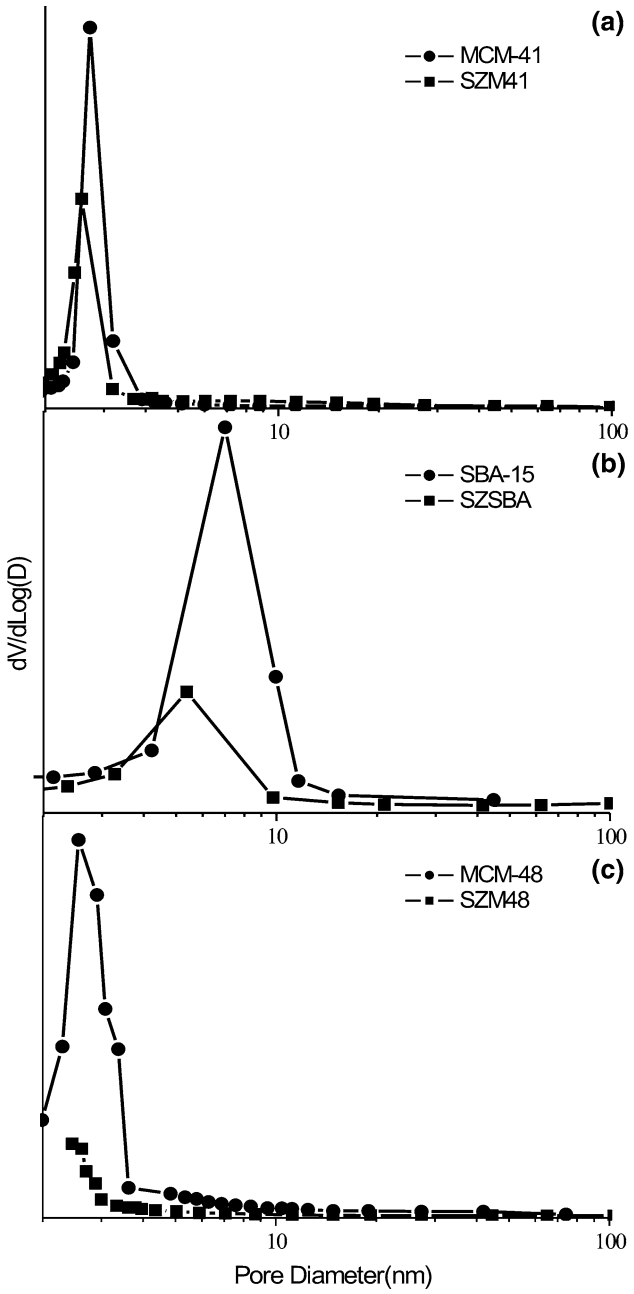

Fig. 2 Pore size distributions curves of plain silica and of catalysts: (**a**) MCM-41/SZM41; (**b**) SBA-15/SZSBA; (**c**) MCM-48/SZM48

nitrogen decreases accompanied with a slight shift of the capillary condensation to smaller values of P/P0, in fact, we observe that BET surface area, very high for MCM-41 sample (1,072 m^2/g), decreases in the SZM41 catalyst (796 m^2/g) accompanied by a diminution of pore size diameter (3.7 for plain MCM-41 to 3.3 in the case of SZM41); both effect can be attributed to the introduction of sulphated zirconia into the mesopores. Although the change of surface area and pore size, the shape of isotherm was retained after SZ introduction showing that the mesoporous morphology of support has been preserved in the SZM41 sample.

Upon nitrogen adsorption, SBA-15 exhibits an irreversible type IV isotherm (Fig. 1b) with a clear type-H2 hysteresis loop that is typical of materials with cylindrical mesopores. The isotherm displays a sharp inflection occurring at relative pressure of: $0.7 < P/P0 < 0.9$, corresponding to the capillary condensation in the mesopores which strongly suggest the presence of large pores (8 nm). The sharpness of this step indicates a uniform and narrow pore size, which is in good agreement with TEM results (see Fig. 6). The introduction of SZ results in a marked change in the shape of hysteresis loop indicating a pore size distribution less ordered and uniform. This hysteresis loop was characteristic for a percolation effect caused by small ZrO_2 particles settling within the mesopores and effectively forming ink-bottle pores [11]. Also for SZSBA the capillary condensation, as observed for SZM41 catalyst, is shifted slightly towards lower partial pressures and the volume of gas adsorbed decreases after introduction of SZ into the mesopores. The BET surface area is around 760 m^2/g for SBA-15 and very smaller in the case of SZSBA catalyst (230 m^2/g). The marked decrease of surface area of SZSBA sample is, maybe, related to the micropores present on the wall of SBA-15 [27, 28]. It is likely that Sulphated Zirconia particles fill the micropores of silica which disappeared after introduction of SO_4^{2-}/ZrO_2. In fact, as shown in Table 1, the consistent micropores volume fraction presents in the plain SBA-15 sample disappear almost completely in the supported catalyst. The pore size distribution is unimodal for both pure and modified materials (Fig. 2b) and a decrease in pore diameter has been revealed in the SZSBA sample (6.2 nm).

Also, MCM-48 sample possess a type IV isotherm (Fig. 1c) that contain an H3 hysteresis loop, as defined by IUPAC, associated with solids with slit-shaped pores or plate like particles with uniform shape and size. Loading of SZ led to a marked change in the shape and size of the isotherm. The hysteresis loop of composite material is larger suggesting a less ordered and uniform pore size distribution which is probably caused by a small inhomogeneous pore filling. The BET surface area of pristine MCM-48 is around 1,234 m^2/g, and a drastic decrease of surface area (156 m^2/g) and of pore volume has been revealed in the SZM48 material, indicating a significant blocking of three-dimensional meso-channel and a partial collapse of mesoporous order during SZ introduction. The pore size distribution of pure silica is narrow (Fig. 2c) and is centered around 3.4 nm while pore size diameter (calculated by the geometric method) of SZM48 is higher than that of plain support (4.5 nm). This phenomenon is, probably, related with the partial destruction of thin pore wall of silica during high temperature calcination (973 K) of

Table 1 Chemical–physical properties of MCM-41 and of SZ promoted systems

Sample	Area BET (m^2/g)	V_{mes} (ml/g)	$V_{micropor}$ (ml/g)	$D_{mes + XRD}$ (nm)	t (nm)	a (nm)	% SO_4^{2-}
MCM-41	1,072	0.77	0.00	3.7	1.01	4.3	0
SZM41	750	0.49	0.00	3.4	1.30	4.7	7.0
SBA-15	767	1.02	0.12	8.0	2.03	9.6	0
SZSBA	228	0.40	0.02	6.2	3.60	9.4	3.7
MCM-48	1,234	0.80	0.07	3.3	0.72	8.7	0
SZM48	156	0.12	0.03	4.5	4.70	18.6	4.2

$Zr(SO_4)_2$/MCM-48 composite that led to formation of larger pores with irregular shape.

Although the reduced amount of physisorbed N_2 and the change of pore diameter revealed after ZrO_2/SO_4^{2-} introduction, all catalysts still show mesoporosity which is indicative of a coating of the inner surface of silica supports rather than a complete filling of the pores. This result is in agreement with literature [16].

The sulphate content, determined by ionic chromatography, is reported in Table 1. After calcination at 973 K, $Zr(SO_4)_2$ decomposes following the reaction $Zr(SO_4)_2 \rightarrow ZrO_2+2SO_3$; however, a small portion of the sulphates remain on the zirconia surface to form the active sulphated zirconia phase. The sulphate content is up of 3 wt.% on all catalysts and SZM41 sample shows the higher sulphate retention (7.0 wt.%).

In order to gain structural information on plain silica materials and on catalysts, X-ray diffraction and transmission electron microscopy measurements were carried out. The attention was focused, especially, on the effect of SZ loading on the periodic arrangement of the pore systems and on the lattice parameters of silica supports.

In Fig. 3 are shown the low 2θ regions of the XRD powder patterns of the studied samples.

The initial MCM-41 system presents the typical XRD pattern of a mono-dimensional hexagonal meso-phase *p6mm* (see Fig. 3a). It exhibits a very intense diffraction peak corresponding to 3.7 nm *d*-spacing and three other well-resolved less intense peaks corresponding to the 2.2, 1.9 and 1.5 nm *d*-spacing. These four peaks can be indexed respectively as the (100), (110), (200) and (210) reflections of the hexagonal structure with a unit cell parameter $a = 2d_{100}/\sqrt{3} = 4.3$ nm. The high intensity and good resolution of XRD peaks, attributed to the regular arrangement of the periodic structure, indicate the high quality of the calcined MCM-41 sample.

The low angle XRD patterns of SBA-15 (Fig. 3b) are characterized by the presence of a prominent peak at 2θ–0.8° and of another weak peak around 2θ–1.8° (that correspond to the 8.3 and 4.3 nm *d*-spacing, respectively, and can be indexed as the (100) and (110) diffractions associated with the 2-D *p6mm* hexagonal symmetry. From the observed reflections the unit cell parameter $a = 2d_{100}/\sqrt{3} = 9.6$ nm, characteristic for the 2-D hexagonal lattice of SBA-15, can be calculated.

The powder XRD patterns of the parent MCM-48 silica (Fig. 3c) shows in the 2θ range 2–6° the typical reflections which can be indexed according with the 3-D cubic space group *Ia3d*. The first intense peak appears at $2\theta = 2.5°$ and represents the (211) plane while the second weaker peak can be indexed as the (332) reflection; the corresponding calculated *d*-spacing are respectively 3.6 and 1.9 nm. The cell edge can be calculated as $a = d_{211}\sqrt{6} = 8.7$ nm (assuming a 3-D cubic geometry).

After impregnation and thermal decomposition of sulphated zirconia precursor [$Zr(SO_4)_2$] on mesopores of silica supports, the XRD patterns exhibit the presence of the characteristic low angle reflections due to the periodic ordered structure of cubic and hexagonal supports; there are, however, some significant differences between the diffraction profiles of catalysts and that of parent supports. As shown in Fig. 3 the relative intensity of X-ray reflections decreases remarkably for all supported samples accompanied by a slight shift to lower values of 2θ in the case of SZM48 and SZM41 materials. The value of the unit cell parameter, *d*-spacing and wall thickness for all samples are reported in Table 1. The values indicate that lattice parameters of SBA-15 sample have not been significantly affected by introduction of the catalytic active phase (SZ). In the case of MCM-41 supported catalysts the slight expansion of the cell parameter from 4.3 to 4.7 nm suggests a small modification of the initial mesoporous lattice while in the case of SZM48 the remarkable variation of the cell parameter from 8.7 to 18.6 nm suggests that in the latter case the initial features of the mesoporous lattice are greatly altered by incorporation of the sulphates species. Also the wall thickness (t) changed after SZ introduction with a considerable increase in particular for SZM48 sample. This increase of wall thickness (corresponding to a decrease of surface area) is probably related to the condensation of SiO_2 and to an increase of connection between SiO_4 tetrahedron groups after calcination of SZ/SiO_2 composites at 973 K. It is reported that the thermal stability of mesostructured materials strongly depend of the texture

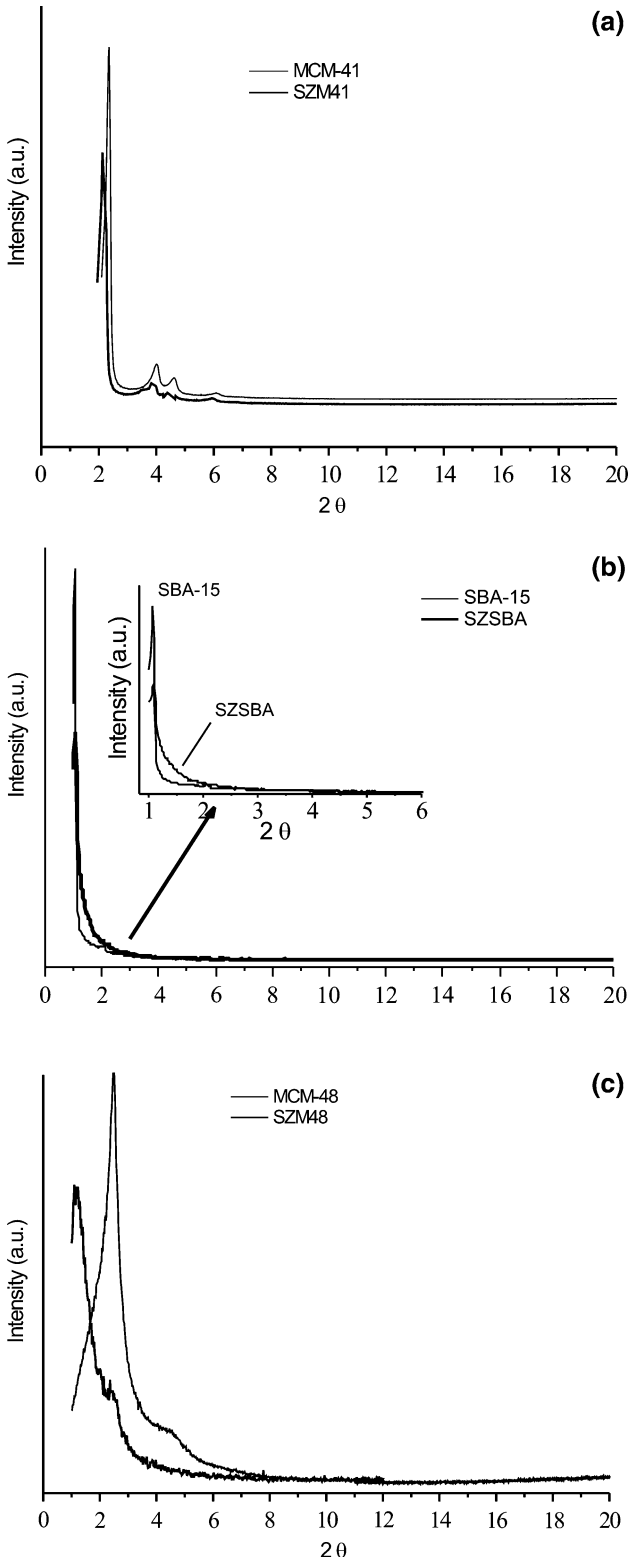

Fig. 3 X-ray powder diffraction patterns in the low 2-theta region of (**a**) MCM-41 and SZM41; (**b**) SBA-15 and SZSBA; (**c**) MCM-48 and SZM48

properties, particularly on the wall thickness of the pores. Therefore, the increasing of the pore wall must enhance the stability of the resulted composites.

For all catalysts a decrease in intensity and a broadening in the low angle XRD peak have been observed suggesting that a degradation of the periodic mesostructure of silica supports might have occurred upon incorporation of the sulphated species. However, according to Sauer et al. [29] the strong reduction of peaks intensity does not, necessary, reflects a collapse of porous order after introduction of sulphated zirconia but could be a result of the increased fraction of incoherently scattered X-rays due to a disordered insertion of zirconia nanocrystals in the modified samples. This consideration suggests that the observed decrease in the intensity of XRD peaks upon SZ introduction can be assigned partly to a decrease in the periodic order but principally to the "lower scattering contrast" due to the presence of zirconia. Note that for SZM48 sample the degradation of mesoporous structure is larger than in the two other composites as denoted by the broad (211) reflection.

In the light of previous diffraction characterization results we suggest that, even if the lattice parameter were affected by the presence of SZ, the ordered structure of all silica supports has been retained to certain degree in all catalysts. This is particularly true in the case of SZM41 and SZSBA samples that maintain a detectable degree of order, whereas in the case of SZM48 the fraction of ordered material as inferred from the XRD pattern can be largely overestimated since the amorphous fraction only contribute to the increase of background noise actually observed in Fig. 3c.

In Fig. 4 are reported the patterns of supported samples recorded in the high 2θ region. They are characterized by very weak and broad peaks, which can be assigned to the presence of the tetragonal and monoclinic ZrO_2 crystalline phases. This suggests that very small SZ particles might have been formed outside the pore structure when the samples were heated at 973 K. Since these particles can be

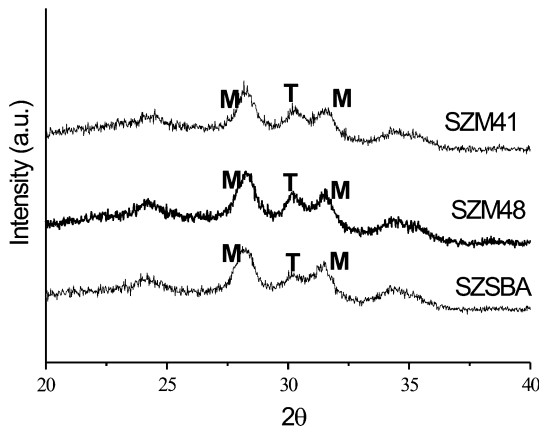

Fig. 4 X-ray powder diffraction pattern in the high 2-theta region: ZrO_2 phase (T, tetragonal phase; M, monoclinic phase)

detected by XRD, the low intensity of zirconia peaks observed in the region of 10–50° implies that the concentration of SZ particles is relatively low, and most of the SZ is highly dispersed on the interior surface of silica supports.

TEM images of the siliceous supports are shown in Figs. 5 and 6. It can be seen that the parent MCM-41 sample (Fig. 5d) is made of submicrometer particles, with a shape mainly spherical but also rod-like. On the contrary, SBA-15 (Fig. 6c, d) is characterized by elongated/platy particles. High magnification TEM images (scale bar, 20 nm) of MCM-41 and of SBA-15 show the existence of both highly ordered hexagonal array and layered structural features. The hexagonal array corresponds to the view of the crystals down to the *c* axis while the layered image is that of the crystal whose *c* axis is parallel to the image plane. Micrographs recorded along the (110) direction (perpendicular to the pore axis) show well-ordered channels with continuous pore walls (Fig. 5a for MCM-41, Fig. 6b for SBA-15); images recorded along the (001) direction (direction of the pore channel axis) clearly exhibit the uniform pore size and the hexagonal arrangement of the porous network (Fig. 5a for MCM-41, Fig. 6a for SBA-15). The pore sizes determined by TEM measurement are in agreement with those obtained from N_2 adsorption and XRD measurement, around 3 nm in the case of MCM-41 sample, 8–9 nm for SBA-15 material. TEM micrographs of catalysts SZM41and SZSBA (Fig. 7), display that the ordered structure of siliceous supports has been preserved after SZ introduction in agreement with XRD analysis. As shown in Fig. 7b (inset A), well resolved interference fringe patterns reveal the presence of ZrO_2 in the mesoporous channels of silica structure; this is also confirmed by EDS analyses.

From examination of the TEM micrograph of sample SZM48 (Fig. 7c) it appears that this material is not ordered which is in contrast with the X-ray diffraction pattern suggesting a rather well ordered cubic structure. Such a discrepancy is readily explained by considering the low stability of M41 samples under the high voltage electron beam [33]. This phenomenon was particularly severe for the parent MCM-48 (TEM images not reported here), probably due to its relatively thin ($\sim$0.7 nm) pore walls.

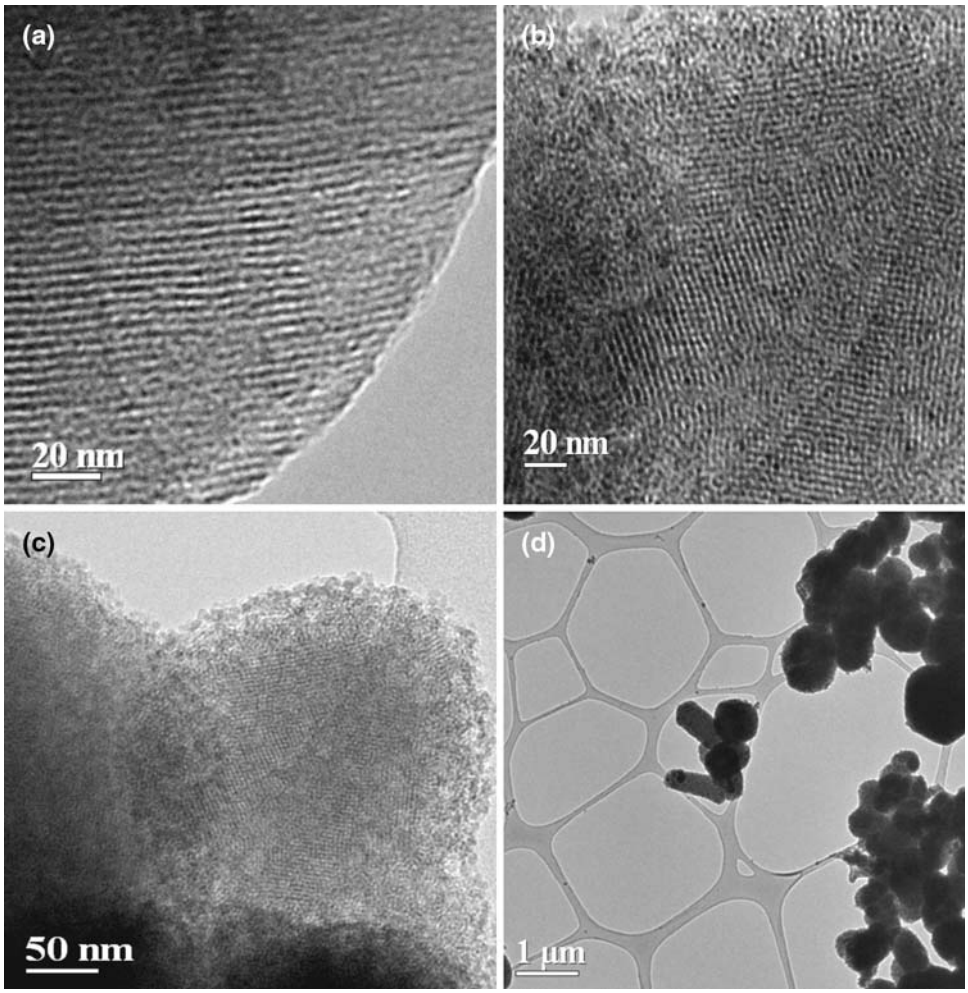

Fig. 5 TEM images of MCM-41 sample: (**a**) micrograph recorded along the direction perpendicular to the pore axis; (**b**) micrograph recorded along the direction of the pore channel axis;; (**c**–**d**) micrographs at low magnification TEM showing the shape of MCM-41 particles

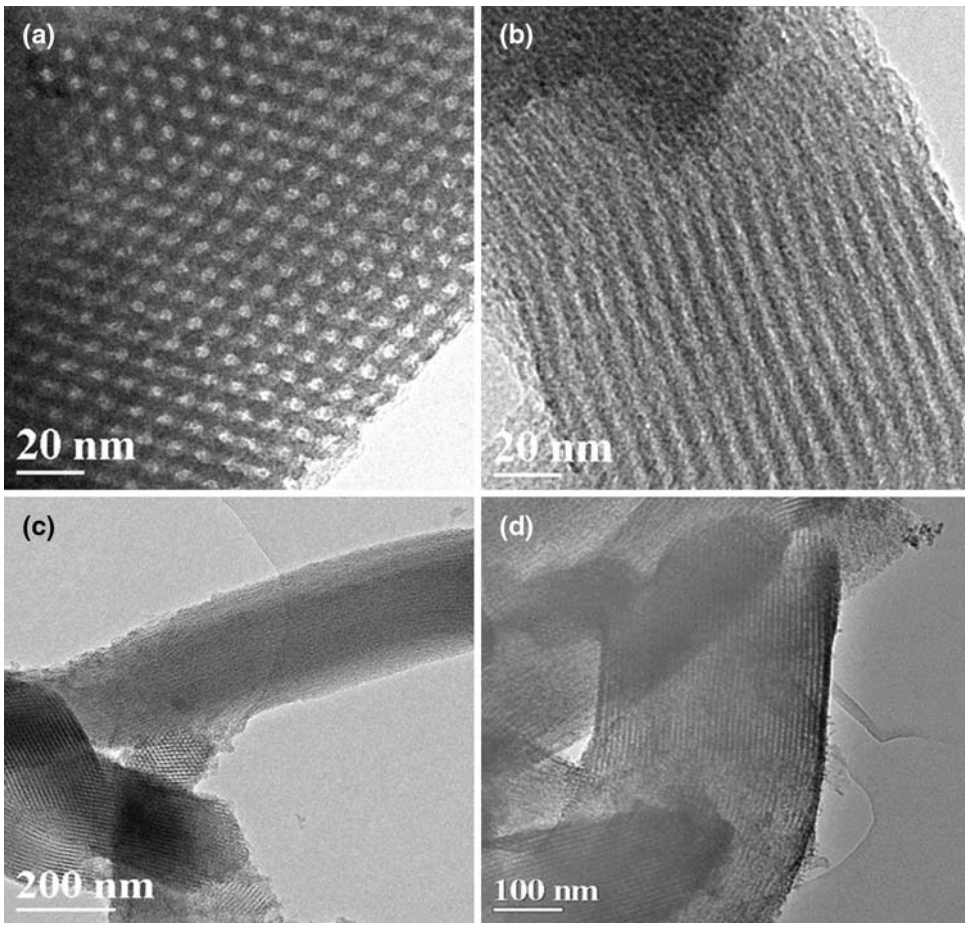

Fig. 6 TEM images of plain SBA-15 sample: (**a**) micrograph recorded along the direction of the pore channel axis; (**b**) micrograph recorded along the direction perpendicular to the pore axis; (**c**–**d**) micrograph at low magnification TEM exhibiting the elongated shape of SBA-15 particles

The principal advantages in the use of ordered mesoporous catalysts are related to their high surface areas, pore volume and narrow-pore size distribution. Our data demonstrate that the morphology and structure of silica porous materials MCM-41 and SBA-15 can be preserved without considerable degradation of pore ordered although the high content of SO_4^{2-}/ZrO_2 (40 wt%) introduced. It is important to note that the surface area of SZ supported catalysts is larger than that of a traditional bulk sulphated zirconia (prepared by precipitation of a zirconium salt), typically around 50–100 m^2/g.

3.2 Catalytic Reaction

The benzoylation reaction of anisole was used as a test reaction to evaluate the potential application of our systems as catalysts in liquid-phase acylation reactions of aromatics.

As know anisole reacts with benzoic anhydride on the catalyst surface to give a mixture of 4- and 2-methoxybenzophenone (2- and 4-MPB) (Scheme 1).

The only GC-detectable side reaction is the decomposition of benzoic anhydride with water to give benzoic acid. This secondary reaction is a critical point for the damage of the catalyst.

Conversion, after 3 h batch reaction, selectivity toward the desired product and yields are reported in Table 2.

It is possible to observe that all catalysts are active in the reaction with good conversions despite the relative bland reaction conditions. The best catalytic performance was exhibited by SZM41 system with a yield value of 55%. These results are quite comparable with that obtained for a standard SZ catalyzed reaction, carried out in the same conditions as reported in the experimental section, with a yield of 60%. Lower isomer yields were obtained, instead, with SZSBA and especially with SZM48 system. It is to note, moreover, that for the last sample (SZM48) the side reaction (decomposition of benzoic anhydride to give benzoic acid) is very marked. In order to get some more information about surface terminations (i.e., functionalities) of the systems of interest FT-IR spectroscopy has been resorted to. We can observe that in a medium high dehydration stage (see Fig. 8) the OH pattern of plain MCM-41 and of SBA-15 samples is only little affected by the presence of the SZ instead in the case of SZM48 system the OH pattern is almost totally upset: the typical ‘‘free’’

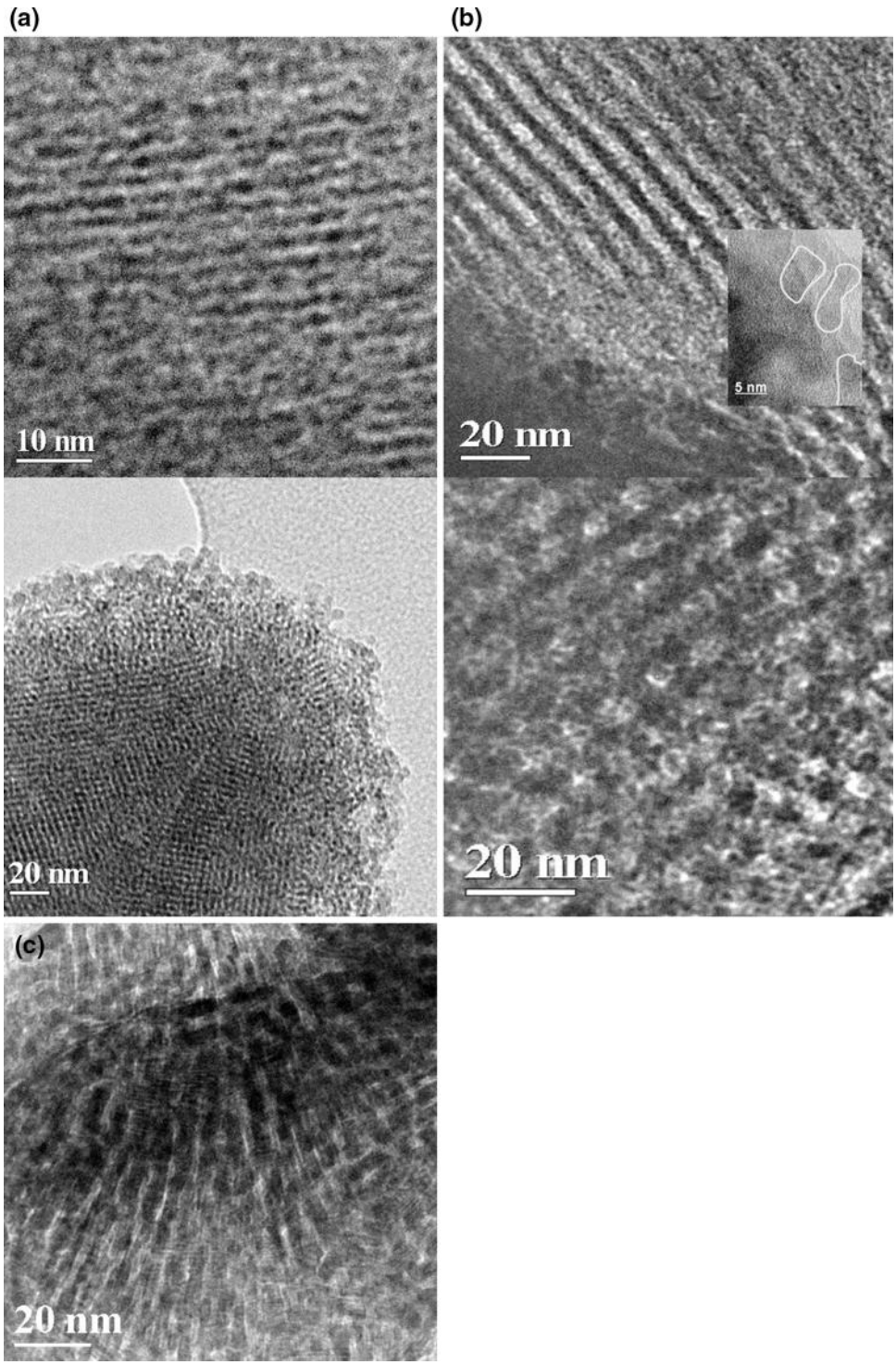

Fig. 7 (**a**) TEM images of SZM41 catalyst; (**b**) TEM images of SZSBA catalyst; (**c**) TEM image of SZM48 catalyst. Inset (A) exhibits a micrograph at higher magnification showing the presence of ZrO_2 in the mesoporous channel of SZSBA sample

Scheme 1

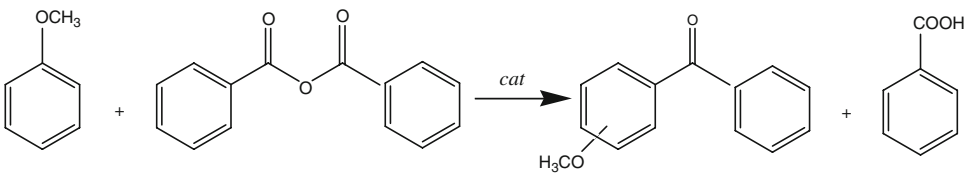

Table 2 Conversion, yield and selectivity of anisole acylation at 3 h for all samples

Sample	Anhydride conversion (%)	Yield Σ MPB (%)	Product distribution (%)	
			2-MPB	4-MPB
SZM41	64	55	1	99 ± 1
SZSBA	58	47	4	96 ± 1
SZM48	54	38	2	98 ± 1

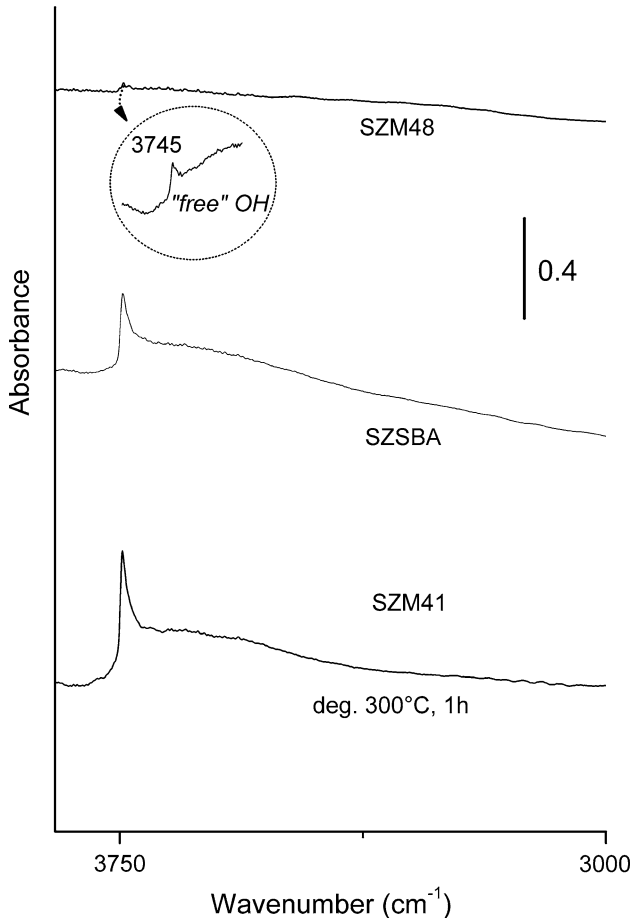

Fig. 8 Absorbance FTIR spectra in the 3,850–3,000 cm^{-1} range (ν_{OH} stretching region)

SiO–H species represents only a secondary feature (3745 cm^{-1}), whereas the envelope due to OH species interacting by H-bonding is now the main component. This result can be probably correlated with the greater formation of benzoic acid in the case of this sample.

To study the recycling of samples, the exhausted catalysts were recovered and reused in the reaction. After 3 h of reaction the catalysts were filtered from the slurry, washed with anisole and dried at 383 K for 1 night. The color of powdered sample appears pink. The used catalysts, as aspect, used in a new catalytic run show a significant decrease of conversion and yield to respect of fresh sample. Deactivation of catalysts is likely due to the presence of organic species (namely, benzoates species) adsorbed on surface during the reaction which are difficult to remove simply by washing with solvents. Carbonaceous residues could be removed by calcination in air at 723 K for 90 min (after the regeneration the sample is white). After this oxidizing treatment the catalytic activity of catalysts could be restored completely and the regenerated SZ supported samples reproduce perfectly yields and conversions of the fresh catalysts (Fig. 9). In the second recycling only a small decrease in the yield of ketones has been detected. This result evidences the main advantage offered by our catalysts if compared with other systems, such as heteropoly acids or Nafion-H: even if they suffer a short initial decrease of activity, supported SZ-based catalysts possess high thermal stability, which permits the removal of deactivating carbonaceous species at rather elevated temperatures without loosing the possibility of recovering the

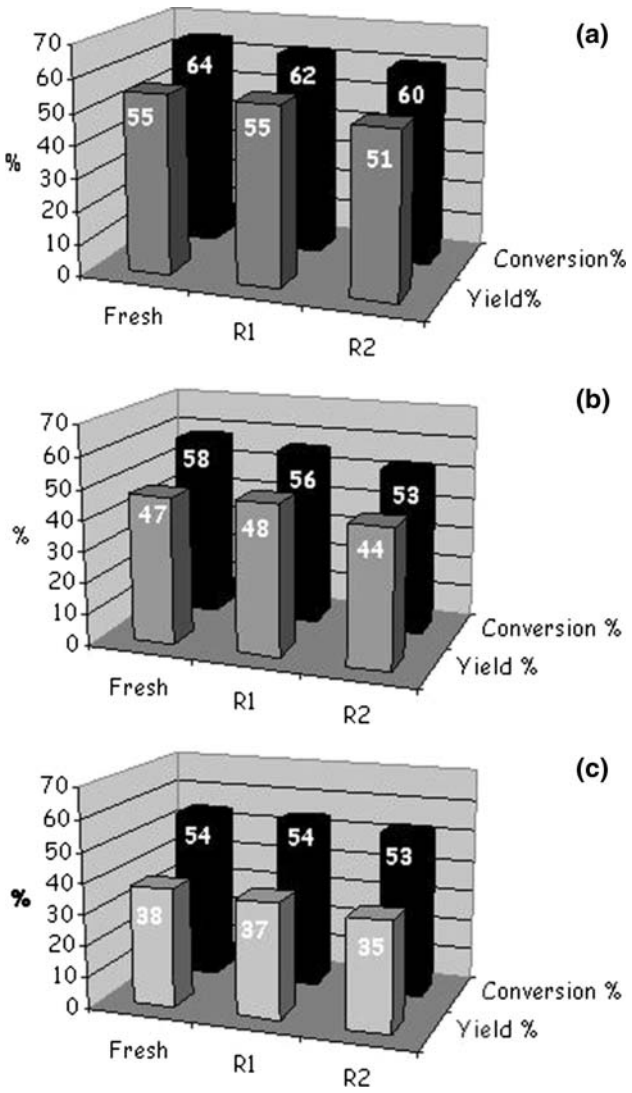

Fig. 9 Reuse of catalysts. Conversions of benzoic anhydride after 3 h and yield of 2- and 4-MPB for SZM41 (**a**), SZSBA (**b**), SZM48 (**c**) samples in the first use (fresh) and in 1° (R1) and 2° reuse (R2)

full catalytic activity. A similar result has been reported, recently, for plain SZ systems [6] but an higher calcination temperature is necessary for the complete restoration of the catalytic activity.

As reported in literature [7, 31], there are close relationships between catalytic activity in liquid phase acylation reactions, surface acidity and textural properties. The surface acidity of samples was studied by FT-IR spectroscopy of absorbed molecules and the obtained results are reported in Fig. 10. Strong Lewis acidity, as revealed by CO adsorption at RT, is present for all SZ-silica samples (Fig. 10a) and only a slight but not significant difference on the frequency vibration of CO has been detected for SZM48 sample (ν_{CO}–2,195 cm^{-1}). The obtained bands can be ascribed to CO molecules interacting with *cus* surface Zr^{4+} cations and despite the low intensity their frequency ($\sim$2,195–2,198 cm^{-1}) is totally similar to that typical of pure sulphated zirconia systems [32]. It is worth noting that, in the case of SZ systems,

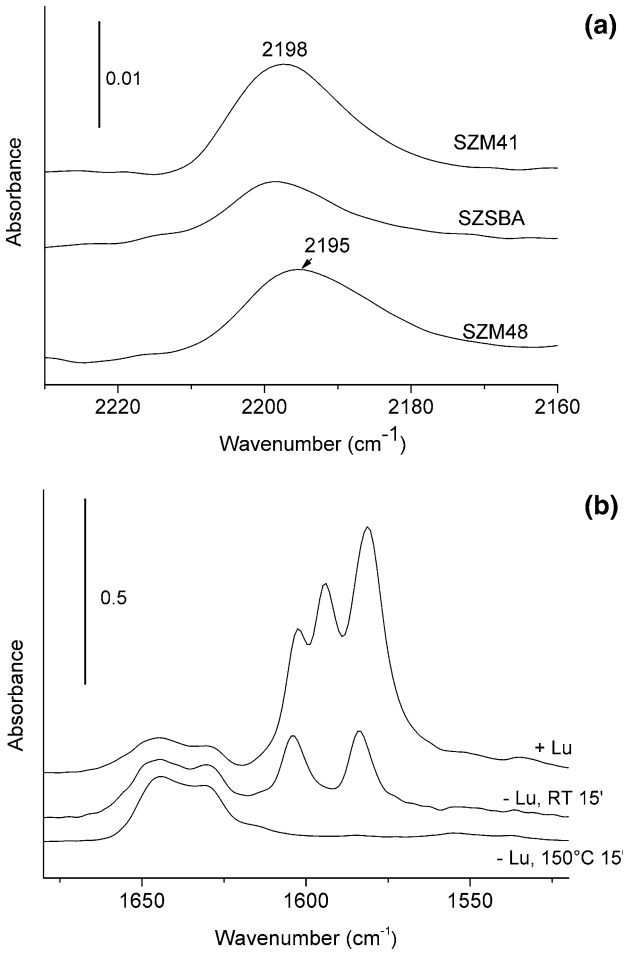

Fig. 10 (**a**) Differential absorbance FT-IR spectra in the *v*CO stretching region of CO adsorbed (pCO $\approx$ 100 Torr) at RT on the various samples; (**b**) The 8a–b ring stretching modes of 2,6-DMP adsorbed/desorbed on all samples activated in vacuo at 673 K

carbonyl species with $\nu > 2{,}190$ cm^{-1} are a direct indication of the presence at the surface of electron-withdrawing species, such as surface sulphate species [33]. The total acidity of medium-high dehydrated systems, it has been tested with the adsorption/desorption of 2,6-dimethylpiridine (2,6-DMP) in the RT-150 °C temperature range. Also in this case no relevant differences have been detected; both types of acidity are present on all our systems has revealed by the presence of the envelopes typical of the two sites of adsorption (Brönsted, $\nu > 1{,}615$ cm^{-1}; Lewis $\nu < 1{,}610$ cm^{-1}). On the basis of obtained results we can conclude that the presence of the different mesoporous supports not brings significant change in the surface acidity (Lewis and Brønsted) of SZ-silica composites. The marked difference in their catalytic behavior can be correlated, therefore, mainly to the textural properties.

Dispersion, high concentration and accessibility of catalytic sites are determinant conditions for a good heterogeneous catalyst. Data reported in Table 1 show that SZ/MCM-41 composite possesses high pore volume and large BET surface area which allows a high number of active sites on its surface. These factor, together with its well ordered structure, can plausibly account for the best catalytic performance (higher yield and conversion) exhibited by this sample. The two other families of materials, SZ/MCM-48 and SZ/SBA-15, are characterized, instead, by a significant decrease of surface area and pore volume after introduction of SZ in silica channel particularly significant for SZM48. Especially in this last system the marked pore blocking and the partial collapse of texture, probably, hinder the diffusion of reagents and products in and out of pores causing its poor catalytic performance. It is well known that among the properties which make a good heterogeneous, beside the presence of active catalytic sites, is the pore structure which must be capable to allow the formations of desired products. Especially in liquid phase reaction, of that considered in this investigation, the selectivity towards the products of industrial interest is a fundamental aspect. As reported in the previous section, all the considered catalysts have retained a quite well ordered pore organization (periodic structure and narrow pore size distribution) of the corresponding pure silica supports. Good selectivity in the desired isomer (4-MPB) exhibited by SZM41 catalyst could be related to its narrow and unimodal pore distribution associated with a suitable pore size dimension (around 3 nm). This result is very significant and it is better than that obtained with a "standard" sulphated zirconia (synthesized by precipitation method) that shows a larger and broader pore size distribution. As reported, in the case of SZSBA sample the selectivity is comparable with that of plain sulphate zirconia. Although its ordered structure, the pore size dimensions of this material (6.2 nm) are to large

to envisage a shape and size selectivity toward reagents and products of molecular dimensions ($\sim$1.5 nm) as that involved in this catalytic process.

Data reported in this section seem to indicate a close correlation between textural properties of studied samples and their catalytic activity showing that morphology (surface area, pore size distribution) and structure of catalysts provide an key roll on directing the course of reaction (yield and selectivity).

The results described in this work showed the possibility of employing these mesoporous systems as potentially active catalysts in liquid phase reaction where size and shape selectivity are fundamental. These materials could be a valid alternative to the commercially used catalysts (e.g. zeolites) especially when large molecules are involved in fine chemical process, in fact their structure and pore size dimensions can be easily tailored in function of the catalytic application.

4 Conclusions

In this work is reported the synthesis and characterization of solid acids with ordered pore structure. A narrow correlation between the nature of mesoporous silica supports and the chemical–physical properties of SZ promoted samples has been detected, demonstrating that is possible easily tailor morphology (surface area and pore size dimension) and structure of a solid acid catalyst by the suitable choice of mesoporous supports.

All samples are found to be active in the reaction at relatively bland conditions, with good conversions and yields. The selectivity over 4-MPB, the desired product, is higher than that of other catalysts tested in the same reaction and in similar conditions. The obtained results make the application of these catalysts suitable in fine chemical processes.

Acknowledgements This research was partly financed with funds from INSTM (Project PRISMA 2002) and from the Italian Ministry MIUR (Project FIRB 2001 RBAU01X7PT). The authors want to thank Prof. Stefano Polizzi (University of Venice) for supplying TEM analysis and Dr. Giuseppina Cerrato (Univeristy of Turin) for the FTIR analyses.

References

1. Kresge CT, Leonowicz ME, Roth WJ, Vartuli J, Beck JS (1992) Nature 359:710
2. Arata K (1990) Adv Catal 37:165
3. Morterra C, Cerrato G, Pinna F, Signoretto M (1995) J Catal 109:157
4. Davis BH, Keogh RA, Srinivasan R (1994) Catal Today 20:219
5. Guo C, Yao S, Cao J, Qian Z (1994) Appl Catal A: Gen 107:229
6. Zane F, Melada S, Signoretto M, Pinna F (2006) Appl Catal A: Gen 299:137
7. Deutsch J, Trunschke A, Müller D, Quaschning V, Kemnitz E, Lieske H (2004) J Mol Catal A 207:51
8. Deutsch J, Prescott HA, Müller D, Kemnitz E, Lieske H (2005) J Catal 231:269
9. Wong MS, Huang HC, Ying JY (2002) Chem Mater 14:1961
10. Janssen AH, Yang CM, Wang Y, Schüth F, Koster AJ, De Jong KP (2003) J Phys Chem B 107:10552
11. Schüth F, Wingen A Sauer J (2001) Micropor Mesopor Mater 44:465
12. Landau MV, Vradman L, Wang X, Titelman L (2005) Micropor Mesopor Mater 78:117
13. Sun Y, Zhu L, Wang R, Lin S, Jiang D, Xiao F-S (2002) Appl Catal A: Gen 21:237
14. Chen CL, Cheng S, Lin HP, Wong ST, Mou CY (2001) Appl Catal A: Gen 215:21
15. Hua W, Yue Y, Gao Z (2001) J Mol Catal 170:195
16. Wang W, Cheng C-L, Xu N-P, Han S, Cheng TLS, Mou C-Y (2002) Catal Lett 83:281
17. Wang W, Wang J-H, Chen C-L, Xu N-P, Mou C-Y (2004) Catal Today 97:307
18. Salas P, Chen LF, Wang JA, Armendáriz H, Guzman ML, Montoya JA, Acosta DR (2005) Appl Surf Sci 252:1131
19. Ghedini E, Signoretto M, Pinna F, Cerrato G, Morterra C (2006) Appl Catal B: Environ 67:24
20. Monnier A, Schuth F, Huo Q, Kumar D, Margolese D, Maxwell RS, Stucky GD, Petroff P, Firouzi A, Janicke M, Chmelka BF (1993) Science 261:1299
21. Zhao D, Feng J, Huo Q, Melosh N, Frederickson GH, Chmelka BF, Stucky GD (1998) Science 279:548
22. Brunauer S, Emmett PH, Teller E (1938) J Am Chem Soc 60:309
23. Galarneau A, Driole M-F, Petitto C, Chiche B, Bonelli B, Armandi M, Onida B, Garrone E, Di Renzo F, Fajule F (2005) Micropor Mesopor Mater 83:172
24. Galarneau A, Desplantier D, Duartre R, Di Renzo F (1999) Micropor Mesopor Mater 27:297
25. Sarzanini C, Sacchero G, Pinna F, Signoretto M, Cerrato G, Morterra C (1995) J Mater Chem 5:353
26. Zhao XS, Lu GQ, Whittaker AK, Millar GJ, Zhu HY (1997) J Phys Chem B 101:6525
27. Kruk M, Jaroniec M, Ko CH, Roo R (2000) Chem Mater 12:1961
28. Roo R, Ko CH, Kruk M, Antochshuk V, Jaroniec M (2000) J Phys Chem B 104:11465
29. Sauer J, Marlow F, Schüt F (2001) Phys Chem Chem Phys 3:367
30. Fröba M, Köhn R, Bouffaud G (1999) Chem Mater 11:2858
31. Signoretto M, Breda A, Somma F, Pinna F, Cruciani G (2006) Micropor Mesopor Mater 91:23
32. Morterra C, Cerrato G, Di Ciero S, Signoretto M, Pinna F, Strukul G (1997) J Catal 165:172
33. Morterra C, Cerrato G, Emanuel C, Bolis V (1993) J Catal 142:349